Nanoscale

Accepted Manuscript

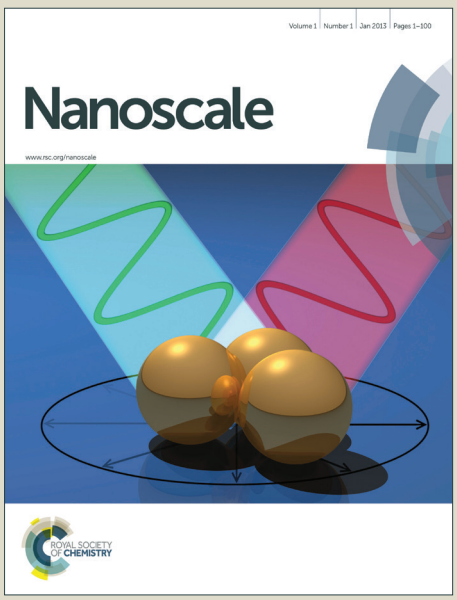

ROYAL SOCIETY OF CHEMISTRY

www.rsc.org/nanoscale

Cite this: DOI: 10.1039/c0xx00000x

www.rsc.org/ xxxxxx

PAPER

Uniform Ni/SiO_2@Au magnetic hollow microspheres: rational design and excellent catalytic performance in 4-nitrophenol reduction

Shenghuan Zhang,[a] Shili Gai,[a] Fei He,[a] Yunlu Dai,[b] Peng Gao*[a], Lei Li,[a] Yujin Chen*[c], and Piaoping Yang*[a]

Received (in XXX, XXX) Xth XXXXXXXXX 20XX, Accepted Xth XXXXXXXXX 20XX
DOI: 10.1039/b000000x

A unique and rational design was firstly presented to fabricate Ni/SiO_2@Au magnetic hollow microspheres (MHMs) with interesting structure and well-dispersed metal nanoparticles. Hierarchical nickel silicate hollow microspheres were firstly synthesized using silica colloidal spheres as a chemical template. Then Ni/SiO_2 MHMs with well-dispersed Ni nanoparticles (Ni NPs) were prepared *via* an in situ reduction approach. Ni/SiO_2@Au MHMs were finally obtained by immobilizing uniform Au nanoparticles (Au NPs) onto Ni/SiO_2 support through a low temperature chemical reduction process. It is found that Ni/SiO_2@Au MHMs inherit the shape and uniformity of the original silica scaffold and Ni NPs and Au NPs with less 5 nm are well dispersed on the mesoprous silica shell with narrow size distribution. Both Ni/SiO_2 and Ni/SiO_2@Au MHMs show excellent catalytic activity in 4-nitrophenol reduction reaction. Importantly, introduction of a little amount of Au NPs onto Ni/SiO_2 MHMs can markedly improve the catalytic activity, and especially Ni/SiO_2@Au MHMs still show high conversion even after re-use for several cycles with magnetic separation. The unique structure, high catalytic performance, and ease of separation make Ni/SiO_2@Au MHMs be high promising in diverse applications.

1. Introduction

With the rapid development of nanoscience and nanotechnology, great attention has been focused on the synthesis of nanosized noble metal particles, such as gold, silver, platinum, and palladium, because of their excellent optical, electronic, and especially catalytic properties.[1–5] Recently, much attention has been paid to the catalysis application of gold nanoparticles (Au NPs) on account of their highly catalytic activity in several catalytic process including catalytic reduction of 4-nitrophenol.[6] However, smaller Au NPs tend to be easy aggregated due to their large surface area-to-volume ratio and hard to be removed from the reaction media result in reducing their application in recycling.[7] Moreover, high cost of Au NPs limits their practical application. Therefore, reducing the used amounts of Au NPs on the condition of maintaining the highly catalytic efficiency is the top priorities. And a common method is to find a suitable multifunctional support to immobilize the Au NPs.

For suitable supports, one would like to have the following properties: a high specific surface area and strong affinity for the catalyst particles so as to immobilize the catalyst particles with well dispersibility, an excellent chemical stability in the operating environment to maintain the good property of catalyst, and other useful properties, such as magnetic, electrical conductivity to achieve the multi-function of the catalyst.[8] Up to now, various solid supports such as carbon nanotube,[9] graphene oxides,[10] polymers,[11] zeolites,[12] metal oxides[13] have been used for immobilizing the metal nanoparticles to enhance their catalytic activity and stability. Among them, silica especially hollow SiO_2 spheres have become a promising candidate for supports due to the large loading capacity and numerous surface Si-OH groups. Up to now, various SiO_2 hollow spheres and silica shell coating metal oxides, especially Fe_3O_4 with magnetic properties, have been synthesized to immobilize noble metal particles.[14–17] However, finding a multifunctional support combined magnetic and catalytic properties is still a challenge.

Except for the noble metal particles, other metal particles, such as nickel, cobalt, and copper, have also been extensively employed as heterogeneous reduction catalysts, because they are much cheaper than noble metal and exhibit good catalytic activity.[18–20] Among them, nickel nanoparticles (Ni NPs) with magnetic property have drawn much attention for the low cost and multifunction.[21,22] Besides, the catalytic activity of Ni NPs is also relatively high.[23–25] From this point of view, a creative idea is experimenting with combination of Au NPs and Ni NPs to provide a better alternative, where Au NPs can be easily separated from the medium by an external magnetic field. Various Ni NPs have been successfully synthesized *via* a number of techniques such as chemical reduction,[26] electrochemical reduction,[27] microwave,[28] and thermal decomposition of organometallic precursor.[29,30] However, the relatively larger particle size and lower uniformity reduce the performance and thus limit the application. Moreover, the formation of Ni NPs by thermal decomposition and reduction from inorganic precursor has rarely been reported.

In this contribution, we proposed a novel method to fabricate highly uniform Ni/SiO_2 magnetic hollow microspheres by an *in situ* thermal decomposition and reduction route. This unique reduction method from nickel silicate precursor can markedly prevent the aggregation and growth of Ni NPs, which is superior to the conventional precipitation and sol-gel routes. To the best of our knowledge, this is first report on the synthesis of Ni/SiO_2 magnetic hollow microspheres with highly dispersed Ni NPs obtained from the nickel silicate precursor. Ni/SiO_2 MHMs were selected as support for loading Au NPs due to their multifunctional properties, such as large surface area, magnetic properties and co-catalytic properties. After modifying the surface of Ni/SiO_2 magnetic hollow spheres with amino groups, Au NPs was linked to the mesoporous surface with good dispersibility and finally, Ni/SiO_2@Au MHMs was obtained. The as-prepared Ni/SiO_2@Au MHMs were employed as reaction catalyst to investigate the catalytic performance in reduction of 4-NP, and the stability of the multifunctional catalyst was also studied.

2. Experimental section

2.1. Synthesis

Synthesis of hollow nickel silicate spheres. Nickel silicate spheres were prepared by using colloidal silica as template through a chemical conversion process. Silica spheres were prepared by a classic Stöber method. Typically, 0.75 mmol of nickel chloride and 10 mmol ammonia chloride were dissolved in 30 mL of deionizer water, and then 1 mL ammonia solution was added under stirring. The color of the solution was transform from light green to deep blue immediately. 0.1 g as-prepared silica colloidal spheres were dispersed homogeneously in 10 mL deionized water. The above two solution were mixed under ultrasonication and then transferred into an autoclave (50 mL) and heated to a temperature of 100 °C for 12 h. After cooling to room temperature, a green precipitate was collected by centrifugation and washed with deionized water and ethanol three times. The nickel silicate hollow spheres were finally obtained after dried at 60 °C for 12 h.

Synthesis of Ni/SiO_2 MHMs. 0.1 g hollow nickel silicate powders were placed in a ceramic boat in the middle of the horizontal tube furnace. The Ni/SiO_2 magnetic hollow microspheres were obtained by heating at 800 °C for 7 h in 5% H_2/N_2 gas. Black power was collected in the ceramic boat at room temperature.

Synthesis of Ni/SiO_2@Au MHMs. Ni/SiO_2 MHMs were modified with amino groups on the surface of SiO_2 through the siloxane linkage of APTES before conjugating to gold nanocrystals. In a typical procedure, 30 mg as-prepared Ni/SiO_2 MHMs were first dispersed in 20 mL isopropanol containing 400 μL of APTES and then stirred for 2 h at 80 °C. The amino-modified nanopatricles were collected by centrifugation, washed with isopropanol twice and finally dispersed in deionized water. Then the amino-modified Ni/SiO_2 MHMs were dispersed in 20 mL aqueous solution containing 10^{-3} M $HAuCl_4$ and 2.5×10^{-4} M tri-sodium citrate. After stirring for 1 h, 600 μL of $NaBH_4$ solution (0.1 M) was added with vigorous stirring. The solution turned to purple immediately after the addition of $NaBH_4$ which indicated the formation of Au NPs. After stirring for another 1 h, the product was collected by centrifugation using a magnet, washed three times with deionized water and ethanol. The final product was designed as Ni/SiO_2@Au magnetic hollow microspheres.

2.2. Catalytic reaction

The reduction of 4-NP by $NaBH_4$ was chosen as the model reaction to investigate the catalytic performance of Ni/SiO_2@Au MHMs. Typically, 1.85 mL ultrapure water, 50 μL 4-NP solution (5 mM) and 1.0 mL freshly as-prepared $NaBH_4$ aqueous (0.2 M) were added into a standard quarts curette, respectively. The solution turned from light yellow to bright yellow immediately after $NaBH_4$ aqueous was added. Subsequently, 4 mg Ni/SiO_2@Au MHMs were added to start the reaction. The color of the mixture gradually vanished, indicating the reduction of the 4-NP. Changes in the concentration of 4-NP were monitored by the UV-vis absorption which were recorded in the scanning range of 250–500 nm at room temperature. For comparison, 4 mg Ni/SiO_2 MHMs and different amount of Ni/SiO_2@Au MHMs were also used as the catalysts for the reduction of 4-NP.

2.3. Characterization

X-ray diffraction (XRD) measurement was examined on a Rigaku D/max-TTR-III diffractometer using monochromatic Cu Kα radiation (λ = 0.15405 nm). Transmission electron microscopy (TEM) and high-resolution transmission electron microscopy (HRTEM) micrographs were performed on a FEI Tecnai G^2 S-Twin transmission electron microscope with a field emission gun operating at 200 kV. N_2 adsorption/desorption were measured at a liquid nitrogen temperature (77 K) using a Micromeritics ASAP 2010 instrument. The specific surface area was obtained by the Brunauer-Emmett-Teller (BET) method, and pore size distribution was calculated from the adsorption branch of the isotherm. Magnetization measurements were performed on a MPM5-XL-5 superconducting quantum interference device (SQUID) magnetometer at 300 K. The absorbance of 4-NP was obtained on a TU-1901 UV-vis spectrophotometer.

3. Results and discussion

The synthetic strategy of Ni/SiO_2@Au MHMs is presented in Scheme 1. The hierarchically hollow structured nickel silicates were synthesized under alkaline condition at high temperature. In alkaline condition, the silica chains on the surface of colloidal silica will be broken by hydroxide at high temperature, then silicate-ion groups are generated and will directly react with nickel ions to form nickel silicate particles *in situ* around the silica cores.[31] And the inner silica chains of the colloidal silica go on dissolving to generate silicate-ion groups until the silica core has been dissolved completely. The Ni/SiO_2 hollow microspheres are then obtained *in situ* decomposition and further reduction in hydrogen atmosphere at high temperature. Finally, the Ni/SiO_2@Au MHMs were obtained by using *in situ* reduction method in the presence of $NaBH_4$.

XRD patterns of the silica template, nickel silicate and Ni/SiO_2 MHMs are shown in Fig. 1, respectively. For silica template, a broad band centered at $2\theta = 22°$ is the characteristic for amorphous SiO_2. For the product after hydrothermal treatment,

Cite this: DOI: 10.1039/c0xx00000x

www.rsc.org/xxxxxx

ARTICLE TYPE

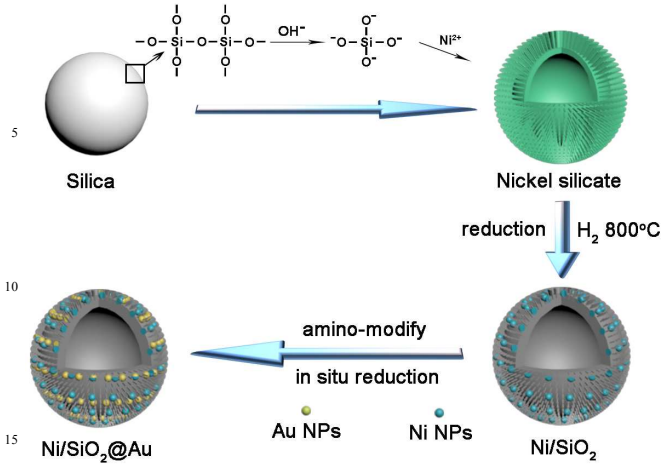

Scheme 1 Schematic illustration of the synthetic procedure for Ni/SiO_2@Au MHMs.

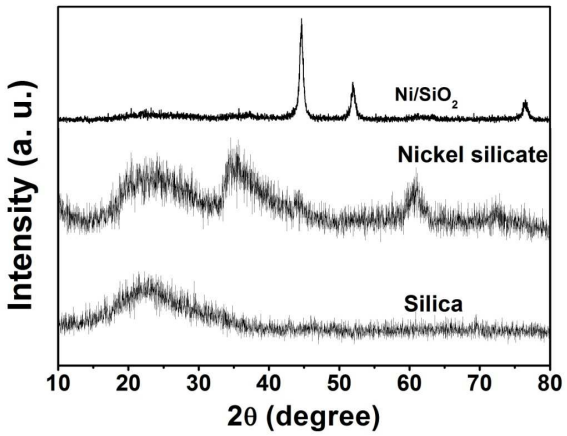

Fig. 1 XRD patterns of colloidal silica spheres, nickel silicate and Ni/SiO_2 hollow spheres.

the diffraction can be indexed to nickel silicate hydrates. In the case of as-prepared Ni/SiO_2 MHMs, it is apparent that all the diffraction peaks can be directly indexed to cubic phased nickel (JCPDS No. 04–0850) in Fm-35 (225) space group, except for a weak broad band at $2\theta = 22°$ assigned to amorphous SiO_2. It is noted that no diffractions related with nickel silicate can be detected, suggesting complete conversion from nickel silicate to Ni/SiO_2 after the reduction process.

The respective TEM images of silica template, nickel silicate, and Ni/SiO_2 are given in Fig. 2. In Fig. 2a for silica template, highly uniform microspheres with the particle size of about 400 nm and smooth surface (Fig. 2b) are obtained. From the TEM image of nickel silicate (Fig. 2c), we can see that the product consists of well-defined hollow microspheres with the diameter of about 600 nm, which is much larger than that of the original silica template. The obvious contrast between the black edge and

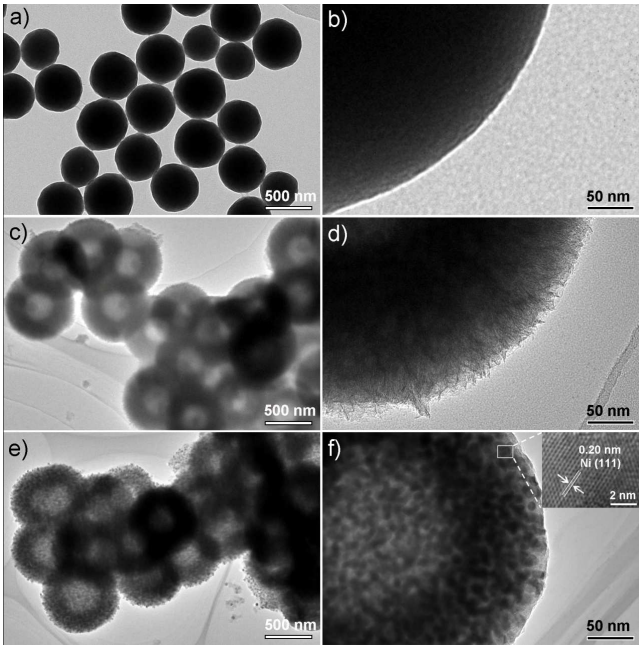

Fig. 2 a) Low-, b) high-magnification TEM images of pure silica; c) low-, d) high-magnification TEM images of nickel silicate; and e) low-, f) high-magnification TEM image of Ni/SiO_2 MHMs.

the pale center confirm the hollow structure. And the uniform shell is about 150 nm in thickness. Close observation reveals that the surface of hollow microspheres becomes coarse, porous and bestrewn, which is composed of numerous thin nanosheets (Fig. 2d). For Ni/SiO_2 MHMs (Fig. 2e, f), the product comprises uniform hollow microspheres with mean size of 600 nm, which is similar to that of nickel silicate microspheres. The results indicate that the size, shape and hollow structure can well be kept after the annealing and reduction procedure. It should be pointed out that compared with nickel silicate spheres, the surface of the hollow spheres is still rough while the laminar sheets almost disappear. Instead, numerous Ni NPs with the particle size of less 15 nm are highly dispersed both on the surface and inside the mesoporous SiO_2 shell. This should be caused by the unique reduction route from uniform nickel silicate precursor, which can efficiently prevent the aggregation and further growth of Ni NPs. In the HRTEM image (inset in Fig. 2f), the obvious lattice fringes confirm the high crystallinity. The distance between the adjacent lattice fringes (marked by the arrows) is determined to be about 0.20 nm, which matches well with the d_{111} spacing of cubic phased Ni.

Fig. 3 shows the XRD patterns of Ni/SiO_2@Au and Ni/SiO_2 MHMs, respectively. It can be seen that except for the diffraction peaks of cubic Ni, two obvious peaks at 38.2° and 64.5° can be assigned to the reflections of the (111) and (220) planes of cubic Au (JCPDS No. 04–0784), respectively. It should be noted that the (200) crystalline plane of cubic Au centers at 44.4° should be

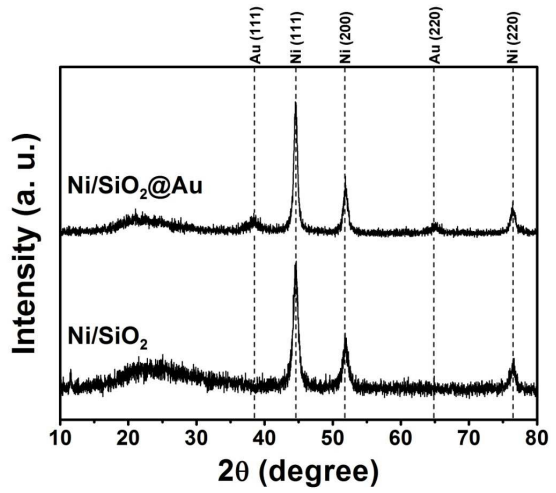

Fig. 3 XRD patterns of Ni/SiO_2 and Ni/SiO_2@Au MHMs.

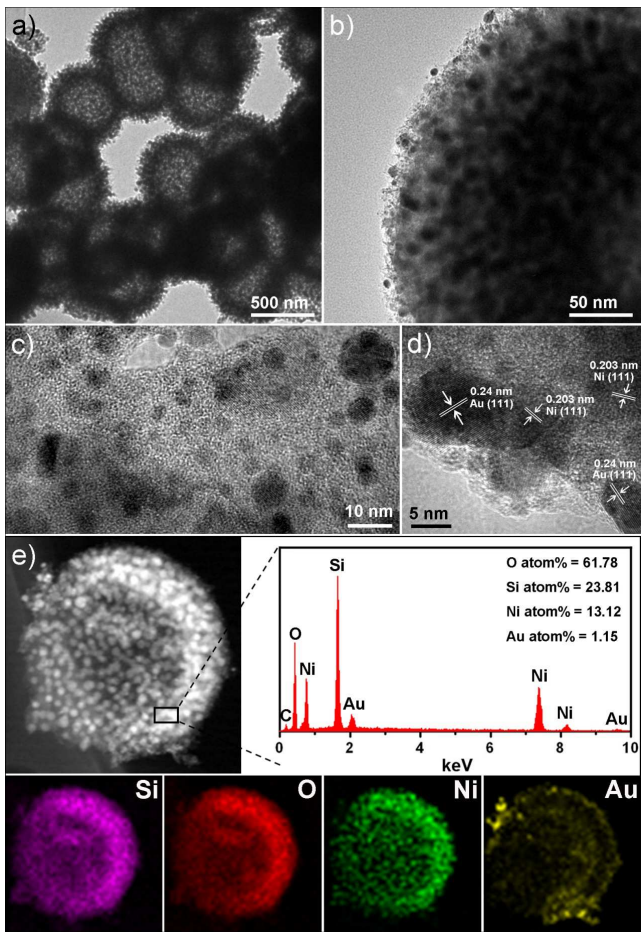

Fig. 4 a) Low-, b) high-magnification TEM images, c, d) HRTEM images, and e) EDS spectrum and mapping of Ni/SiO_2@Au composite.

covered by the (111) crystalline plane of cubic Ni centered at 44.5°.

From the TEM image (Fig. 4a), we can see that Ni/SiO_2@Au maintains the uniform size and hollow structure of original Ni/SiO_2 MHMs. In the magnified TEM image of a partial

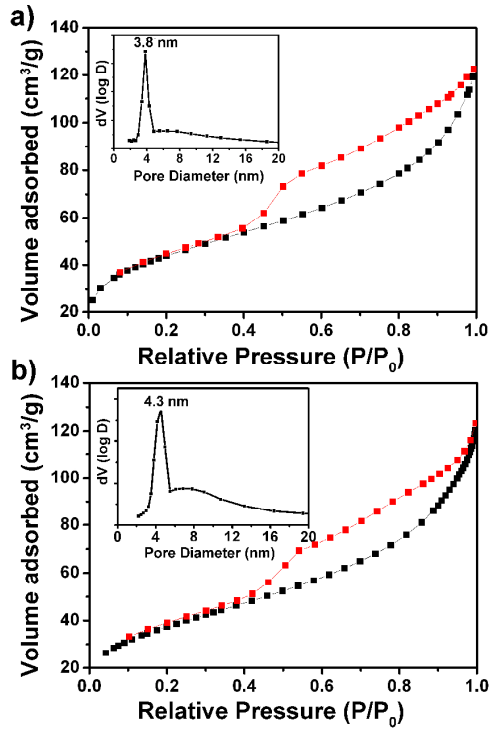

Fig. 5 N_2 adsorption/desorption isotherm of Ni/SiO_2 (a) and Ni/SiO_2@Au (b), the corresponding pore size distribution (inset).

Ni/SiO_2@Au particle (Fig. 4b), besides the uniformly dispersed Ni NPs with particle size of 15 nm, some tiny nanoparticles with diameter of about 5 nm assigned to Au NPs can also be found, which is further confirmed by magnified TEM image (Fig. 4c). As shown, some tiny nanoparticles with obvious lattice fringes are well dispersed on the surface of silica. In the HRTEM image (Fig. 4d), the distance of 0.24 nm between the adjacent lattice fringes agree well with the d_{111} interplannar spacing of cubic Au (JCPDS No. 04–0784), while the distance of 0.20 nm matches well with the d_{111} spacing of cubic Ni (JCPDS No. 04–0850). In the EDS of Ni/SiO_2@Au (Fig. 4e), the Si, O, Ni and Au elements can be detected. It is clear that the silicon, oxygen, and nickel elements are uniformly dispersed on the silica shell. In addition, the small gold nanocrystals with smaller size are also apparent, which disperse uniformly on the surface of the silica spheres.

N_2 adsorption/desorption isotherm and the corresponding pore size distribution (inset) of Ni/SiO_2 MHMs and Ni/SiO_2@Au are shown in Fig. 5. Both the nitrogen adsorption/desorption can be classified as type IV isotherm with a small Hysteresis loop. The obvious step at the relative pressure (p/p_0) between 0.4 and 0.6 indicates that the existence of the mesopores. The BET surface area and average pore size are calculated to be 152 cm^2/g and 3.78 nm for Ni/SiO_2 (inset in Fig. 5a). The high specific surface area and the mesoporous shell suggest that Ni/SiO_2 MHMs is a good candidate as support to load active Au NPs. From Fig. 5b, we can see the specific surface area and average pore size distribution almost remain the same after immobilizing Au NPs on Ni/SiO_2 MHMs, indicating there are little effects of Au loading on the specific surface area and pore size distribution of Ni/SiO_2@Au.

Cite this: DOI: 10.1039/c0xx00000x

www.rsc.org/xxxxxx

ARTICLE TYPE

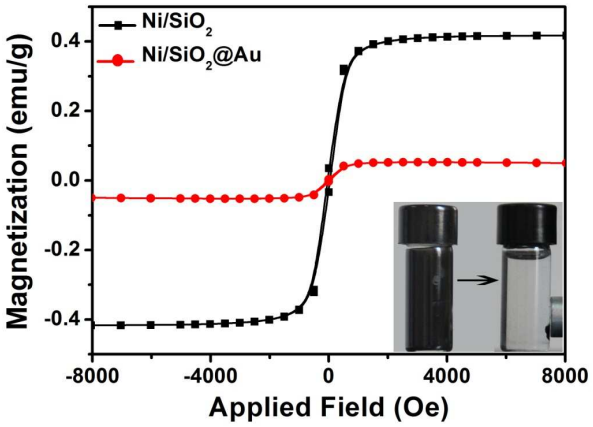

Fig. 6 Magnetization curves of Ni/SiO_2 and Ni/SiO_2@Au. The inset is the photograph for the magnetic separation.

In Fig. 6, the magnetic hysteresis loops of the two samples measured at room temperature show nearly no remanence or coercivity, suggesting the quasi-superparamagnetic nature. For the particles below the critical size (30 nm for Ni particles), superparamagnetic behavior can be achieved at room temperature because of the higher thermal fluctuation energy compared with anisotropic energy.[32] However, a small hysteresis loop can be observed due to the non-magnetic silica support. The magnetizations (M_s) of the Ni/SiO_2 MHMs is determined to be 0.4 emu/g, which is smaller than that of bulk nickel metal at room temperature.[33] It is reasonable that because the small size of Ni will be accompanied with the increase in the specific surface and the crystal lattice defects.[25] It should be noted that after immobilizing Au NPs, the product still exhibits quasi-superparamagnetic property. The photograph of the magnetic separation demonstrates the easy manipulation of Ni/SiO_2@Au MHMs by an external magnetic field, which is very important for the recycling of the catalysts after the reaction.

It is well known that 4-aminophenol (4-AP) is an important intermediate for the manufacture of analgesic and antipyretic drugs, while 4-NP is the most common organic pollutions in the industrial and agricultural waste water.[34–38] The conversion of 4-NP to 4-AP over noble metal nanoparticles has been widely investigated for the degradation of 4-NP and the efficient production of 4-AP. Therefore, the catalytic reduction of 4-NP with an excess amount of $NaBH_4$ was chosen as a model reaction to evaluate the catalytic performance of Ni/SiO_2@Au MHMs. In Fig. 7a, the absorption peak at 317 nm is assigned to pure 4-NP, which exhibits light yellow under neutral and acidic conditions (inset in Fig. 7a). The peak shifts to 400 nm after adding an aqueous solution of $NaBH_4$, the colour changes to bright yellow for the formation of 4-nitrophenolate ion,[39] and the absorption peak at 295 nm is 4-AP which is colourless after the complete reduction.[40] Fig. 7b gives the concentration (Ct at time t) to its initial value C_0 (C/C_0) verse reaction time for the reduction of

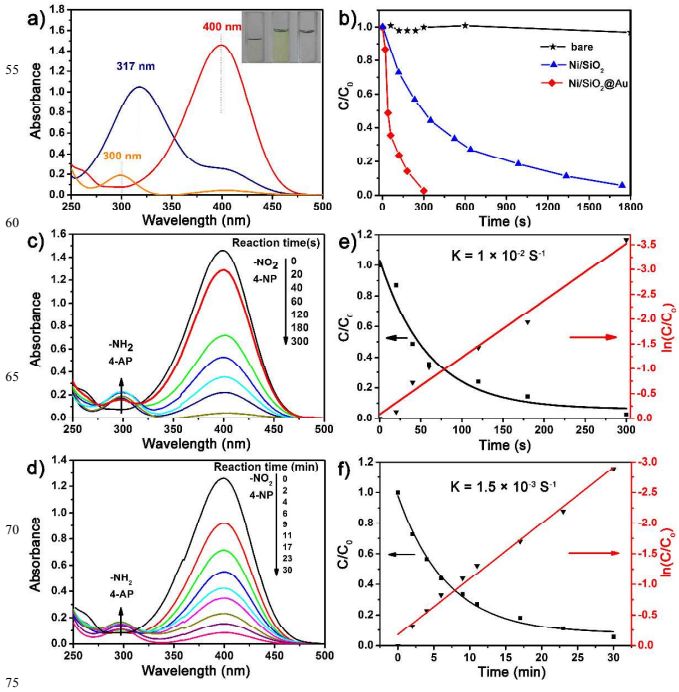

Fig. 7 a) UV-vis absorption spectra of 4-AP and 4-NP before and after adding $NaBH_4$; b) C/C_0 verse reaction time for the reduction of 4-NP at the peak position of 4-NP (400 nm) using bare solution (black line), Ni/SiO_2 (red line) and Ni/SiO_2@Au (red line) as catalysts; c) successive reduction of 4-NP using Ni/SiO_2@Au as catalyst; d) successive reduction of 4-NP using Ni/SiO_2 as catalyst for comparison; e) C/C_0 and $\ln(C/C_0)$ verse reaction time for the reduction of 4-NP over Ni/SiO_2@Au NPs. The ratio of 4-NP concentration (Ct at time t) to its initial value C_0 is directly represented by the relative intensity of the respective absorption peak at 400 nm; f) C/C_0 and $\ln(C/C_0)$ verse reaction time for the reduction of 4-NP over Ni/SiO_2 catalyst.

4-NP with and without catalysts at the peak position of 400 nm. It is obvious that when adding Ni/SiO_2@Au MHMs, the absorbance at 400 nm decreases rapidly within 300 s, which is markedly shorter than that (30 min) of Ni/SiO_2 MHMs. Notably, there is little on the change in absorbance at 400 nm within 30 min without catalysts, confirming that the reduction reaction does not proceed without catalysts. In Fig. 7c, after Ni/SiO_2@Au MHMs is introduced, the absorption intensity of 4-NP at 400 nm significantly decrease with reaction time, while a new peak at 295 nm ascribed to 4-AP appears. Clearly, the peak related with 4-NP almost disappear after 300 s. For comparison, the time-dependent UV-vis absorption spectra over Ni/SiO_2 MHMs are displayed in Fig. 7d. The catalytic reduction time over Ni/SiO_2 MHMs is increased to 30 min, which is much larger than the Au NPs introduced sample. When the initial concentration of the $NaBH_4$ solution is very high, it can be considered as a constant throughout the whole reduction process. Therefore, the reduction rate is assumed to be independent of the $NaBH_4$ concentration, and a pseudo first-order kinetic equation can be applied to evaluate the catalytic rate.[41,42] Because the absorbance of 4-NP is

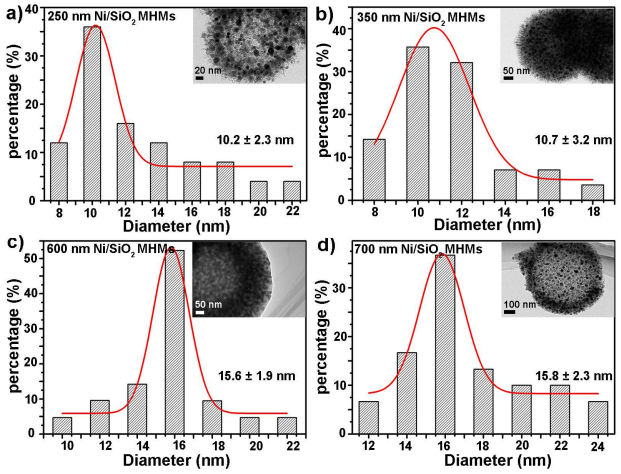

Fig. 8 Size distribution histogram of the Ni NPs calculated from a single Ni/SiO_2 MHMs with the diameter of a) 250 nm, b) 350 nm, c) 600 nm, and d) 700 nm.

proportional to its concentration in the medium, linear relationship between $\ln(C/C_0)$ and reaction time can be considered as the relationship between $\ln(A/A_0)$ and reaction time. Linear relationship between $\ln(C/C_0)$ and the reaction time by using Ni/SiO_2@Au MHMs as catalyst is displayed in Fig. 7e, which matches well with the first-order reaction kinetics. The rate constant k is calculated to be 1×10^{-2} s^{-1}, which is much higher than those reported Au, Ag, Pt and Pd catalysts on different kinds of supports.[15,16,43–45] Additionally, for comparison, linear relationship between $\ln(C/C_0)$ and the reaction time by using Ni/SiO_2 MHMs as catalyst is given in Fig. 7f, which still matches well with the first-order reaction kinetics. The rate constant k is calculated to be 1.5×10^{-3} s^{-1}, which is much smaller than that (1×10^{-2} s^{-1}) of Ni/SiO_2@Au. However, it is still higher than the reported Ni supported catalysts or Ni based composite material (Ni@Au).[46–48] This should be due to the unique reduction approach induced good dispersion of active Ni NPs on/in the hollow mesoporous silica. In particular, the catalytic activity can be significantly improved by immobilizing a small amount of Au NPs on the surface of the supported Ni catalysts, which should also be attributed to the good dispersion and small particle size (5 nm) of Au NPs.

The catalytic mechanism for 4-nitrophenol reduction relies on the electrons from the BH_4^- donor to the acceptor 4-NP. In aqueous medium, BH_4^- ions are adsorbed on the surface of catalyst. After electron transfer (ET) to the metal nanoparticles, the hydrogen atom forms from the hydride, then attacks 4-NP molecules to reduce it. This ET induced hydrogenation of 4-NP occurred spontaneously. It is also reported that metal nanoparticles play a role in storing electron after ET from the hydride.[49] And whether Au NPs or Ni NPs, the catalytic mechanism is the same except for the catalytic activity. Furthermore, SiO_2@Au catalyst is synthesized following the similar capping method. And the TEM image of SiO_2@Au is displayed in Fig. S1. The diameter of Au NPs is about 5 nm with high dispersion on the surface of SiO_2 spheres. Fig. S2 gives the UV-vis absorption spectra of successive reduction of 4-NP using

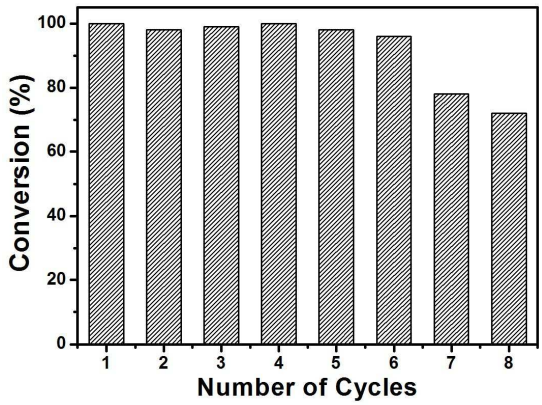

Fig. 9 The reusability of Ni/SiO_2@Au MHMs as a catalyst for the reduction of 4-NP with $NaBH_4$.

SiO_2@Au as catalyst. The absorbance at 400 nm decreases rapidly within 540 s which is longer than that of Ni/SiO_2 MCMs (in 300s). Although the specific surface area SiO_2@Au is much different from Ni/SiO_2@Au, the loading amount of Au NPs is the same according to the ICP data. Therefore, it is possible that there is synergistic catalytic effect between Ni and Au.

The catalytic activity of the catalysts is affected by the diameter of Ni NPs. Therefore, Ni NPs with different diameter have been controllably synthesized. And Fig. 8 shows the size distribution histogram of the Ni NPs calculated from a single Ni/SiO_2 MHMs of different diameter. It clearly reveals that with the increasing of the diameter of Ni/SiO_2 MHMs, the diameter of Ni NPs increases either. The catalytic activity of Ni/SiO_2@Au with various sizes is displayed in Fig. S3. The catalytic reduction time increases from 120 s to 480 s with the size of Ni NPs (from 10 nm to 16 nm). This can be account for the decrease of the active surface area of the Ni NPs with the increase of the size of the catalysts.

Another advantage of Ni/SiO_2@Au catalyst prepared here is the stability and ease to recycle, because the magnetic catalyst can easily be separated by an externally magnetic field. Fig. 9 shows the reusability of Ni/SiO_2@Au catalysts for the reduction of 4-NP with $NaBH_4$. It is obvious that the catalyst still exhibits high catalytic activity even after running for more than eight cycles. The Ni/SiO_2@Au catalyst can be reused and recycled for more than six times with a stable conversion of 95% within 300 s, indicating the high stability. The slight decrease of the conversion with further recycle times should be due to the gradual leaching of Au and Ni NPs with repeated magnetic separation and the covering of 4-AP on the surface, which can been confirmed by the ICP data (Table S1) of the Ni/SiO_2@Au MHMs before and after catalytic reaction for 8 cycles. All these results clearly indicate the high catalytic performance should be attributed to the small particle size, good dispersion of Ni and Au NPs and high specific surface area of the support (silica hollow microspheres).

4. Conclusion

In summary, a highly efficient catalyst, based on well-dispersed distribution of small Au NPs assembled on the surface of Ni/SiO_2 magnetic hollow microspheres was successfully fabricated by an *in-situ* reduction on self-template derived hierarchical nickel

Cite this: DOI: 10.1039/c0xx00000x

www.rsc.org/xxxxxx

ARTICLE TYPE

silica hollow microspheres, followed by a further attaching and reduction procedure of Au NPs. The as-prepared Ni/SiO_2@Au catalysts exhibit excellent catalytic activity and stability for reduction of 4-NP, and especially the magnetic properties make it easy to be recycled. This synthetic strategy provided a useful idea for fabrication of a novel kind of noble metal supported catalyst with high specific surface area and hollow structure, which should be highly promising in diverse catalytic reactions.

Acknowledgements

Financial supports from the National Natural Science Foundation of China (NSFC 21271053), Research Fund for the Doctoral Program of Higher Education of China (20112304110021), Natural Science Foundation of Heilongjiang Province (LC2012C10), Harbin Sci.-Tech. Innovation Foundation (RC2012XK017012), and the Fundamental Research Funds for the Central Universities of China are greatly acknowledged.

Notes and references

a College of Material Science and Chemical Engineering, Harbin Engineering University, Harbin 150001, P. R. China. E-mail: yangpiaoping@hrbeu.edu.cn; gaopeng@hrbeu.edu.cn

b State Key Lab of Rare Earth Utilization Resource, Changchun Institute of Applied Chemistry, Chinese Academy of Sciences, Changchun, 130021

c College of Chemistry, Harbin Normal University, Harbin, China

E-mail: chenyujin@hrbeu.edu.cn

† Electronic Supplementary Information (ESI) available: TEM images of SiO_2@Au, UV-vis absorption spectra of successive reduction of 4-NP using SiO_2@Au as catalysts, C/C_0 verse reaction time for the reduction of 4-NP at the peak position of 4-NP (400 nm) using Ni/SiO_2@Au catalysts with different sizes. See DOI: 10.1039/b000000x

1 N. Tian, Z. Y. Zhou, S. G. Sun, Y. Ding and Z. L. Wang, *Science* 2007, **316**, 732.

2 M. D. Hughes, Y. J. Xu, P. Jenkins, P. McMorn, P. Landon, D. I. Enache, A. F. Carley, G. A. Attard, G. J. Hutchings and F. King, *Nature* **2005**, **437**, 1132.

3 Y. Xia, Y. Xiong, B. Lim and S. E. Skrabalak, *Angew. Chem. Int. Ed.* 2009, **48**, 60.

4 H. Lee, S. E. Habas, S. Kweskin, D. Butcher, G. A. Somorjai and P. D. Yang, *Angew. Chem. Int. Ed.* 2006, **45**, 7824.

5 M. Schrinner, M. Ballauff, Y. Talmon, Y. Kauffmann, J. Thun, M. Möller and J. Breu, *Science* 2009, **323**, 617,.

6 Z. W. Seh, S. Liu, S.-Y. Zhang, K. W. Shah and M.-Y. Han, *Chem. Commun.* 2011, **47**, 6689.

7 A. S. K. Hashmi and G. J. Hutchings, *Angew. Chem. Int. Ed.* 2006**, 45**, 7896.

8 R. Lv, T. Cui, M. S. Jun, Q. Zhang, A. Cao, D. S. Su, Z. Zhang, S. H. Yoon, J. Miyawaki, I. Mochida and F. Kang, *Adv. Funct. Mater.* 2011, **21**, 999.

9 H. Chu, J. Wang, L. Ding, D. Yuan, Y. Zhang, J. Liu and Y. Li, *J. Am. Chem. Soc.* 2009, **131**, 14310.

10 G. Goncalves, P. A. A. P. Marques, C. M. Granadeiro, H. I. S. Nogueira, M. K. Singh and J. Grácio, *Chem. Mater.* 2009, **21**, 4796.

11 T. Ishida and M. Haruta, *Angew. Chem. Int. Ed.* 2007, **46**, 7154.

12 L. Chen, J. Hu, R. Richards, *J. Am. Chem. Soc.* 2008, **131**, 914.

13 X. Chen, H. Y. Zhu, J. C. Zhao, Z. T. Zheng and X. P. Gao, *Angew. Chem. Int. Ed.* 2008, **47**, 5353.

14 J. Zheng, Y. Dong, W. Wang, Y. Ma, J. Hu, X. Chen and X. Chen, *Nanoscale* 2013, **5**, 4894.

15 B. Liu, W. Zhang, H. Feng and X. Yang, *Chem. Commun.* 2011, **47**, 11727.

16 Z. Zhang, C. Shao, P. Zou, P. Zhang, M. Zhang, J. Mu, Z. Guo, X. Li, C. Wang and Y. Liu, *Chem. Commun.* 2011, **47**, 3906.

17 T. Yao, T. Cui, X. Fang, F. Cui and J. Wu, *Nanoscale* **2013**, *5*, 5896.

18 J. Park, E. Kang, S. U. Son, H. M. Park, M. K. Lee, J. Kim, K. W. Kim, H. J. Noh, J. H. Park, C. J. Bae, J. G. Park and T. Hyeon, *Adv. Mater.* 2005, **17**, 429.

19 W. Zhu, J. Ren, X. Gu, M. U. Azmat, G. Lu and Y. Wang, *Carbon* 2011, **49**, 1462.

20 G. J. P. Britovsek, M. Bruce, V. C. Gibson, B. S. Kimberley, P. J. Maddox, S. Mastroianni, S. J. McTavish, C. Redshaw, G. A. Solan, S. Stromberg, A. J. P. White and D. J. Williams, *J. Am. Chem. Soc.* 1999, **121**, 8728.

21 A. C. Johnston-Peck, J. Wang and J. B. Tracy, *ACS Nano* 2009, **3**, 1077.

22 A. El-Gendy, E. M. M. Ibrahim, V. O. Khavrus, Y. Krupskaya, S. Hampel, A. Leonhardt, B. Buechner and R. Klingeler, *Carbon* 2009, **47**, 2821.

23 M. Raula, M. H. Rashid, S. Lai, M. Roy and T. K. Mandal, *ACS Appl. Mater. Interfaces* 2012, **4**, 878.

24 S. Senapati, S. K. Srivastava, S. B. Singh and H. N. Mishra, *J. Mater. Chem.* 2012, **22**, 6899.

25 D. Chen, J. Li, C. Shi, X. Du, N. Zhao, J. Sheng and S. Liu, *Chem. Mater.* 2007, **19**, 3399.

26 M. Han, Q. Liu, J. He, Y. Song, Z. Xu and J. Zhu, *Adv. Mater.* 2007, **19**, 1096.

27 Y.-P. Sun, H. W. Rollins and R. Guduru, *Chem. Mater.* 1999, **11**, 7.

28 C. Parada and E. Morán, *Chem. Mater.* 2006, **18**, 2719.

29 J. S. Bradley, B. Tesche, W. Busser, M. Maase and M. T. Reetz, *J. Am. Chem. Soc.* 2000, **122**, 4631.

30 T. O. Ely, C. Amiens, B. Chaudret, E. Snoeck, M. Verelst, M. Respaud and J.-M. Broto, *Chem. Mater.* 1999, **11**, 526.

31 Y. Wang, G. Wang, H. Wang, C. Liang, W. Cai and L. Zhang, *Chem.-Eur. J.* 2010, **16**, 3497.

32 F. J. Himpsel, J. E. Ortega, G. J. Mankey and R. F. Willis, *Adv. Phys.* 1998, **47**, 511.

33 K. V. Shafi, A. Gedanken, R. Prozorov and J. Balogh, *Chem. Mater.* 1998, **10**, 3445.

34 J. Guo, K. S. Suslick and *Chem. Commun.* 2012, **48**, 11094.

35 Q. Sun, C.-Z. Guo, G.-H. Wang, W.-C. Li, H.-J. Bongard and A.-H. Lu, *Chem.-Eur. J.* 2013, **19**, 6217.

36 R. Abu-Reziq, H. Alper, D. S. Wang and M. L. Post, *J. Am. Chem. Soc.* 2006, **128**, 5279.

37 S. Wunder, F. Polzer, Y. Lu, Y. Mei and M. Ballauff, *J. Phys. Chem. C* 2010, **114**, 8814.

38 M. Zhu, C. Wang, D. Meng and G. Diao, *J. Mater. Chem. A*, 2013, **1**, 2118.

39 J. Liu, G. Qin, P. Raveendran andY. Ikushima, *Chem.-Eur. J.* 2006, **12**, 2131.

40 C.-H. Liu, X.-Q. Chen, Y.-F. Hu, T.-K. Sham, Q.-J. Sun, J.-B. Chang, X. Gao, X.-H. Sun and S.-D. Wang, *ACS Appl. Mater. Interfaces* 2013, **5**, 5072.

41 N. Pradhan, A. Pal and T. Pal, *Langmuir* 2001, **17**, 1800.

42 K. Hayakawa, T. Yoshimura, K. Esumi, *Langmuir* 2003, **19**, 5517.

43 J. Wang, X. B. Zhang, Z. L. Wang, L. M. Wang, W. Xing and X. Liu, *Nanoscale* 2012, **4**, 1549.

44 B. K. Barman and K. K. Nanda, *Chem. Commun.* 2013, **49**, 8949.

45 Y. Mei, Y. Lu, F. Polzer, M. Ballauff and M. Drechsler, *Chem. Mater.* 2007, **19**, 1062.

46 Z. Ji, X. Shen, G. Zhu, H. Zhou and A. Yuan, *J. Mater. Chem.* 2012, **22**, 3471.

47 S. Sarkar, A. K. Sinha, M. Pradhan, M. Basu, Y. Negishi and T. Pal, *J. Phys.Chem. C* 2011, **115**, 1659.
48 R. Xu, T. Xie, Y. Zhao and Y. Li, *Nanotechnology* 2007, **18**, 055602.
49 J.-P. Deng, W.-C. Shih and C.-Y. Mou, *T J. Phys.Chem. C* 2007, **111**, 9723-9728.